Peripheral Zone Prostate Cancer in Patients with Elevated PSA Levels and Low Free-to-Total PSA Ratio: Detection with MR Imaging and MR Spectroscopy[1]

Joan C. Vilanova, MD, PhD
Josep Comet, MD, PhD
Carles Barceló-Vidal, PhD
Joaquim Barceló, MD
Eugeni López-Bonet, MD
Albert Maroto, MD, PhD
Montse Arzoz, MD
Àngel Moreno, PhD
Joan Areal, MD

Purpose: To retrospectively assess the value of endorectal magnetic resonance (MR) imaging and MR spectroscopy combined with the free-to-total prostate-specific antigen (PSA) ratio for detecting prostate cancer in men with elevated PSA levels.

Materials and Methods: The institutional review board approved the study, and all patients provided informed written consent. Endorectal MR imaging and MR spectroscopy were performed in 54 patients with PSA levels greater than 3 ng/mL but less than 15 ng/mL and free-to-total PSA ratio of less than 20%, followed by sextant biopsy in the peripheral zone. For each patient, MR imaging and MR spectroscopic findings, PSA level, and free-to-total PSA ratio were analyzed and compared with biopsy results and/or histopathologic tumor maps with regard to a sextant-modified distribution. The likelihood of cancer in each sextant according to MR and MR spectroscopic findings was graded independently on a scale of 1 (benign) to 5 (malignant). Detection accuracy and a multivariate logistic regression analysis were used to determine the most accurate combination of imaging, and clinical tests were used to detect prostate cancer according to the area under the receiver operating characteristic curve (AUC).

Results: The model incorporating MR imaging, MR spectroscopy, and free-to-total PSA ratio (AUC = 97.5%) was significantly more accurate in predicting prostate cancer than models using MR imaging alone (AUC = 85.1%; $P = .007$), MR spectroscopy alone (AUC = 87.2%; $P = .041$), or MR imaging and free-to-total PSA ratio combined (AUC = 90.8%; $P = .038$).

Conclusion: MR and MR spectroscopy combined with free-to-total PSA ratio improves the predictive value for prostate cancer detection.

[1] From the Department of Magnetic Resonance, Clínica Girona, Lorenzana 36, 17002 Girona, Spain (J.C.V., J.B.); Department of Radiology, Hospital St. Caterina, Salt, Girona, Spain (J.C.V., J.B.); Departments of Urology (J.C.), Pathology (E.L.B), and Radiology (A. Maroto), Hospital Dr J. Trueta, Girona, Spain; Department of Computer Science and Applied Mathematics, University of Girona, Girona, Spain (C.B.V.); Department of Urology, Hospital Germans Trias i Pujol, Badalona, Spain (M.A., J.A.); and CETIR Grup Mèdic, Barcelona, Spain (A. Moreno). Received November 18, 2008; revision requested December 23; revision received February 12, 2009; accepted March 13; final version accepted April 27. Supported by the Generalitat de Catalunya grant 006/30/02 of the Catalan Agency for Health Technology Assessment and Research. **Address correspondence to** J.C.V. (e-mail: *kvilanova@comg.cat*).

The methods most commonly used to detect prostate cancer are digital rectal examination and serum prostate-specific antigen (PSA) levels. Both methods provide suboptimal accuracy for prostate cancer diagnosis. The specificity of PSA levels is poor for PSA levels below 10 ng/mL. About 22%–40% of biopsy-proved prostate cancers manifest with PSA level of less than 4 ng/m, and 70%–80% of patients with PSA level greater than 4 ng/mL do not have prostate cancer (1,2). Thus, between 60% and 75% of men with PSA levels greater than 4 ng/mL undergo unnecessary biopsy (3). Moreover, men can have elevated PSA levels and undergo multiple transrectal ultrasonographic (US)-guided biopsies with negative findings before a diagnosis of cancer is established.

Combined endorectal magnetic resonance (MR) imaging and MR spectroscopy of the prostate has yielded accurate results for prostate sextant localization (4–6). The accuracy of MR spectroscopy for prostate cancer sextant localization is similar to that of biopsy and is greater than that of biopsy in the prostate apex (4).

There have been attempts to improve the specificity of PSA levels. Recently, measurements of molecular isoforms of PSA in the serum, such as the free-to-total PSA ratio or complex PSA, have been investigated. In men with a total PSA level between 3 and 10 ng/mL, use of free-to-total PSA ratio is better in distinguishing prostate cancer from benign disease than the measurement of total PSA level alone (7). A systemic review and meta-analysis confirmed that the use of free-to-total PSA ratio in men with a PSA level between 2 and 10 ng/mL reduces the number of unnecessary biopsies, while maintaining a high cancer detection rate (8).

We aimed to assess the value of endorectal MR imaging and MR spectroscopy combined with free-to-total PSA ratio for detecting prostate cancer in men with elevated PSA levels.

Advance in Knowledge

- In a multivariate analysis, the model combining endorectal MR imaging and MR spectroscopy with free-to-total prostate-specific antigen (PSA) ratio showed a 97% accuracy according to the area under the receiver operating curve, which significantly improved ($P < .05$) early detection of prostate cancer in patients with high levels of PSA and low free-to-total PSA ratio in comparison with using each variable alone.

Implications for Patient Care

- MR imaging and MR spectroscopy may be useful in the diagnostic algorithm to detect prostate cancer in patients with PSA levels greater than 3 ng/mL but less than 15 ng/mL and free-to-total PSA ratio of less than 20% and could potentially prevent unnecessary biopsies.
- The addition of MR spectroscopy to MR imaging can improve detection of prostate cancer.

Materials and Methods

Subjects

Our institutional review board approved this retrospective study, and informed consent was obtained from all patients. Between June 2004 and September 2006, 54 consecutive men (mean age, 60 years; range, 50–71 years) with PSA levels greater than 3 ng/mL but less than 15 ng/mL and free-to-total PSA ratio of less than 20% were selected by the urology department to undergo MR imaging at least 3 weeks before undergoing transrectal US-guided sextant biopsy. The interval between MR imaging examination and biopsy was 13 days ± 8 (standard deviation) (range, 5–35 days). Our flow diagram for patient selection is summarized in Figure 1. Exclusion criteria were prior biopsy, poor general health contraindicating biopsy and/or prostatectomy, previous diagnosis of acute prostatitis, history of prostate cancer, and contraindications to MR imaging (eg, cardiac pacemakers, intracranial clips) or to endorectal coil insertion (eg, anorectal surgery, inflammatory bowel disease). Our primary selection included 61 patients. From these patients, seven were excluded because pathologic data were unavailable ($n = 4$) or there was image distortion ($n = 3$). Blood samples for measuring PSA levels and free-to-total PSA ratio were obtained before digital rectal examination and were always processed at the same laboratory. Prostates with asymmetries, indurations, or nodules were classified as abnormal. Data collected from each patient included digital rectal examination findings, PSA level, and free-to-total PSA ratio.

MR Imaging Technique

MR studies were performed with a 1.5-T whole-body MR imaging unit (version 12.0, Signa Horizon; GE Medical Systems, Milwaukee, Wis). A body coil was used for excitation, and a pelvic four-channel phased-array coil in combination with a commercially available balloon-covered expandable endorectal coil (Endo ATD; Medrad, Pittsburgh, Pa) was used for signal reception. The endorectal coil was positioned with the patient in recumbent lateral position and was insufflated with 80–100 mL of air by a radiologist (J.C.V.) with more than 12 years of experience in prostate

Published online before print
10.1148/radiol.2531082049

Radiology 2009; 253:135–143

Abbreviations:
AUC = area under the ROC curve
Cho = choline
Cit = citrate
Cr = creatine
PSA = prostate-specific antigen
ROC = receiver operating characteristic

Author contributions:
Guarantors of integrity of entire study, J.C.V., J.C., C.B.; study concepts/study design or data acquisition or data analysis/interpretation, all authors; manuscript drafting or manuscript revision for important intellectual content, all authors; approval of final version of submitted manuscript, all authors; literature research, J.C.V., J.C., A.M.; clinical studies, all authors; statistical analysis, C.B.; and manuscript editing, J.C.V., J.C., C.B., J.B., E.L.B., A.M., M.A.

Authors stated no financial relationship to disclose.

MR imaging. We performed transverse T1-weighted sequences with the following parameters: repetition time msec/echo time msec, 500/12; section thickness, 5 mm; intersection gap, 1 mm; field of view, 24 cm; matrix, 256 × 192; transverse frequency encoding; and one signal acquired of the pelvic region from the aortic bifurcation to the symphysis pubis. We performed transverse and coronal high-resolution T2-weighted fast spin-echo imaging of the prostate and seminal vesicles with the following parameters: 5000/102; echo train length, 16; section thickness, 3 mm; intersection gap, 0 mm; field of view, 14 cm, matrix 256 × 192; anteroposterior frequency encoding; and three signals acquired.

MR Spectroscopy

MR spectroscopy data were acquired within a volume around the prostate after reviewing the transverse T2-weighted images. The point-resolved spatially localized spectroscopy box was positioned on transverse T2-weighted images by an MR imaging technologist with the supervision of a radiologist (J.C.V., with more than 12 years of experience in prostate spectroscopy).

Three-dimensional MR spectroscopy data were acquired by using a water- and lipid-suppressed double spin-echo point-resolved spatially localized spectroscopy sequence optimized for the quantitative detection of choline (Cho) and citrate (Cit). To achieve water and lipid suppression, a band-selective inversion with gradient dephasing technique was used. Outer voxel saturation pulses were also used to eliminate signals from the adjacent tissues, especially periprostatic lipids and rectal wall tissue. The line width at half height of the water resonance through the selected volume was used as index of good magnetic field homogeneity. It was automatically calculated by the system and was not greater than 15 Hz as recommended by the manufacturer for volumes below 58 cm^3. No examinations were discarded because of inadequate magnetic field homogeneity. The three-dimensional MR spectroscopy datasets were acquired as 16 × 8 × 8 phase-encoded spectral arrays (1024 voxels), a spatial resolution of 0.24–0.34 cm^3, 1000/130, and 19-minute acquisition time. The total examination time, including coil placement, patient positioning, MR imaging, and MR spectroscopy, was 50–60 minutes.

The three-dimensional MR spectroscopy data were processed and aligned (A.M., with 14 years of experience in spectroscopic imaging) with the corresponding MR image on a workstation (Functool, GE Medical Systems) using specific commercially available software for analyzing three-dimensional MR spectroscopy studies. Spectra were automatically postprocessed, quantified, and reconstructed with such specific software. Peak areas for Cho, creatine (Cr), and Cit were calculated by using numeric integration. Metabolic maps of Cho plus Cr–to-Cit ratio (hereafter, [Cho + Cr]/Cit) were generated. Signal-to-noise ratios were automatically calculated as the ratio between Cit or Cho peak amplitude and the standard deviation of the noise over the 0.40–0.96-ppm range. Voxels were considered suitable if they consisted of at least 75% peripheral zone tissue, did not include periurethral tissue or ejaculatory ducts, had signal-to-noise ratio of greater than 5:1, and were not spectroscopically contaminated by insufficient water or fat suppression.

Image Interpretation

Three faculty radiologists (J.C.V., J.B., A.M., with 12, 6, and 4 years experience in both prostate MR imaging and MR spectroscopic imaging interpretation, respectively) evaluated in consensus all the MR and MR spectroscopy findings, while blinded to the clinical findings. Reader 1 (J.C.V.) had interpreted at least 1500 prostatic MR and MR spectroscopy images, reader 2 (J.B.) had interpreted approximately 200 prostatic MR and MR spectroscopy images, and reader 3 (A.M.) had interpreted approximately 150 prostatic MR and MR spectroscopy images. To allow for direct comparison between MR and three-dimensional MR spectroscopy, only sections covered at three-dimensional MR spectroscopy were evaluated on the MR images.

For tumor localization, the prostate was split along the midline and further divided into the apex, the middle, and base of the gland. Thus, in each case, the prostate was divided into six regions. The imaging evaluation consisted of two parts. First, the three readers interpreted and scored the T2-weighted images using a five-point scale. The presence of cancer on T2-weighted images, identified as an area of low signal intensity within the peripheral zone, was recorded for each region on a standardized form developed for this study. Readers graded their confidence that cancer was present in each region on a five-point scale: Grade 1 indicated definitely no tumor; 2, probably no tumor; 3, tumor possible; 4, tumor probable; and 5, tumor definitely present.

Figure 1

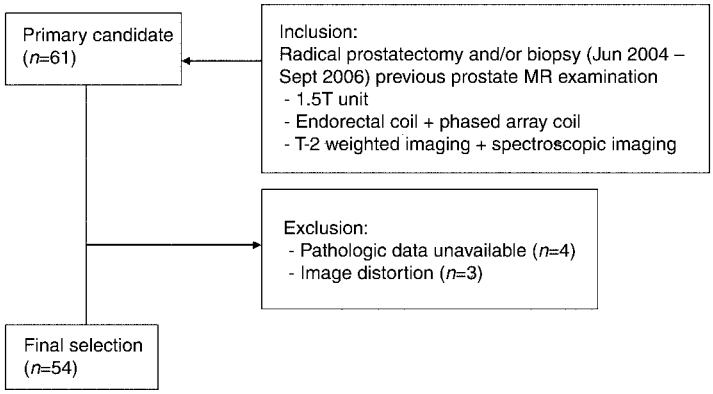

Figure 1: Flow diagram of patient selection.

Second, all MR spectroscopy data were read at least 3 weeks after the first MR data sets. All readers interpreted randomly and independently the MR and MR spectroscopy data sets.

All the voxels within each of the six regions of the prostate were judged, and each region was scored on a five-point scale. To define the five categories, we used mean values of the (Cho + Cr)/Cit ratio calculated from the mean ratio previously published for healthy prostate tissue (9). The (Cho + Cr)/Cit ratio was also categorized on a five-point scale.

A score of 1 was assigned to voxels with a (Cho + Cr)/Cit ratio of less than 0.5; score of 2, voxels with a ratio of 0.5 or greater but less than 0.6; score of 3, voxels with a ratio of 0.6 or greater but less than 0.7; score of 4, voxels with a ratio of 0.7 or greater but less than 0.8; and score of 5, voxels with ratio of 0.8 or greater.

Biopsy

After standard preparation, all patients underwent transrectal US-guided biopsy by using a US scanner (Allegra; Siemens, Erlangen, Germany) with a 6.5-MHz sector probe. Eight prostatic cores were obtained by using an 18-gauge biopsy needle (Bard Urological, Covington, Ga) with a spring-loaded biopsy gun (Manan Medical Products, Northbrook, Ill). Prostatic cores were obtained from the six regions of the peripheral gland, and two additional cores were obtained from the transitional zone on each side of the gland. All cores were labeled according to their sextant topographic location as the base, midgland, or apex from each side of the gland and the transitional zone. All biopsies were performed by one radiologist (A.M.) who was unaware of the clinical and imaging findings. Cores from the transitional zone were not analyzed in this study.

Standard of Reference

Histopathologic material was analyzed by a pathologist (E.L.B.) with 19 years of experience in prostate disease. The material for histopathologic analysis was the biopsy core in 43 patients and the prostatic gland after prostatectomy in 11 patients. The histopathologic analysis included determination of the number of positive cores for prostate cancer. The biopsy or specimen analysis was performed according to the six regions that each prostate was divided in the peripheral gland on the basis of the schematic diagram described previously. Alignment of the imaging data and histopathologic evaluation is considered difficult (10). Thirteen patients with prostate cancer were treated with radiation therapy or androgen ablation. All 30 patients with negative findings at biopsy were followed up for a 6–12-month period. The corresponding data from those patients are being evaluated in order to detect the possible false-negative biopsy results, and further results will be forthcoming.

Statistical Analysis

The sensitivity, specificity, and diagnostic accuracy of the binary variable digital rectal examination were determined by using two dichotomized ratings: positive, when suspicious for cancer, and negative, when not suspicious for cancer.

The diagnostic power of the continuous variables, PSA level and free-to-total PSA ratio, was evaluated by using the area under the receiver operating characteristic (ROC) curve (AUC). Findings of MR and MR spectroscopy were analyzed by considering the prostate as the unit of statistical analysis. For this reason, the maximum value of the six readings on the peripheral sextants was considered the MR imaging (or MR spectroscopy) score for each prostate. The overall diagnostic performance of MR imaging and MR spectroscopy prostate scores from the five-point scale was calculated from the AUC of the corresponding ROC curves. The sensitivity, specificity, and accuracy of MR imaging and MR spectroscopy prostate scores were also calculated by dichotomizing the scores: scores of 3–5 were considered to indicate presence of prostate cancer, whereas scores of 1–2 were considered to indicate not cancerous prostate.

We also evaluated the predictive performance for different combinations of the three predictive variables: MR imaging (five-point scale), MR spectroscopy (five-point scale), and free-to-total PSA ratio. Those analyses were performed by fitting a binary logistic regression model to sample data by using those combinations of variables as predictor variables.

Table 1

Prostate Tumor Detection with Use of PSA Levels, Free-to-Total PSA Ratio, MR Imaging, and MR Spectroscopy

Imaging Modality	Sensitivity (%)	Specificity (%)	Accuracy (%)
PSA level	. . .	. . .	66.8 (52.1, 81.6)
Free-to-total PSA ratio	. . .	. . .	82.5 (71.2, 93.8)
MR imaging (dichotomized)	70.8 (50.6, 91.1)	80.0 (64.0, 96.0)	75.9 (63.6, 88.3)
MR spectroscopic imaging (dichotomized)	87.5 (72.2, 100)	93.3 (82.7, 100)	90.7 (82.1, 99.4)
MR imaging (five-point scale)	. . .	. . .	85.1 (75.7, 94.6)
MR spectroscopic imaging (five-point scale)	. . .	. . .	87.2 (76.2, 98.3)
MR imaging (five-point scale) + MR spectroscopic imaging (five-point scale)	. . .	. . .	94.9 (89.8, 99.9)
MR imaging (five-point scale) + free-to-total PSA ratio	. . .	. . .	90.8 (83.3, 98.4)
MR spectroscopic imaging (five-point scale) + free-to-total PSA ratio	. . .	. . .	95.1 (89.8, 100)
MR imaging (five-point scale) + MR spectroscopic (five-point scale) + free-to-total PSA ratio	. . .	. . .	97.5 (94.3, 100)

Note.—Numbers in parentheses are 95% confidence intervals. The accuracies of predictive models using PSA levels, free-to-total PSA ratio, and MR imaging (five-point scale) and MR spectroscopic imaging (five-point scale) scores are AUCs.

Radiology

Figure 2

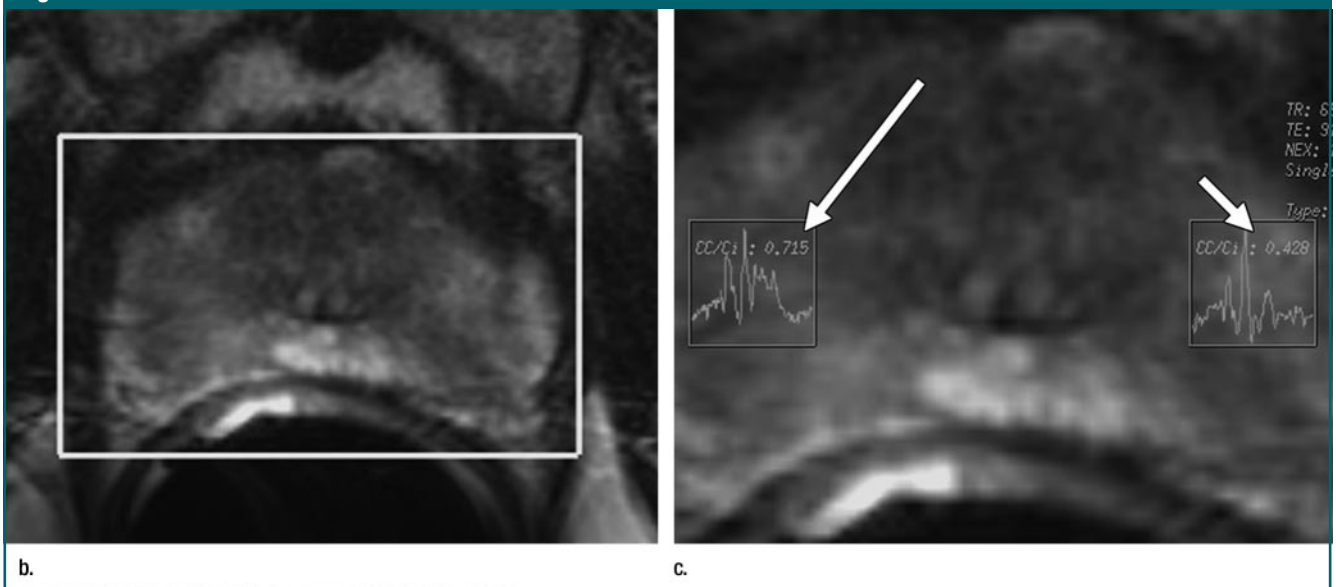

Figure 2: Prostate cancer in 60-year-old man with positive MR spectroscopy results and negative MR results and negative digital rectal examination findings (PSA level, 13.26 ng/mL; free-to-total PSA ratio, 14.92%). **(a)** Photomicrograph from postprostatectomy specimen of the right midgland shows prostate cancer as small irregular glands separated and lined by a single cell layer. (Hematoxylin-eosin stain; reduced from original magnification of ×400.) **(b)** Transverse T2-weighted (6500/91) MR image shows a slight diffuse low signal intensity (boxed area) with linear characteristics without mass effect corresponding to probably no tumor. **(c)** Corresponding three-dimensional ^{1}H MR spectroscopic data from the right midgland (1000/30) shows elevated (Cho + Cr)/Cit *(CC/Ci)* ratio that is suspicious for cancer (long arrow). The voxel from the left side shows normal low (Cho + Cr)/Cit ratio (short arrow).

Despite the ordinal nature of MR and MR spectroscopy scores, these variables were considered numerical in the regression models. The estimated probabilities given by those regression models were used to draw the corresponding ROC curves and to estimate its predictive accuracy from the AUCs.

The data were also analyzed by using another statistical approach based on generalized estimated equations methodology. Instead of considering the maximum value of the six readings of the variables MR and MR spectroscopy on the peripheral sextants for each prostate, individual readings were preserved. Because these individual readings were correlated, it was necessary to introduce a working correlation matrix into the generalized linear model. The correlation structures used in the predictive logistic models were exchangeable and unstructured. Once we estimated the probability of cancer in each of the sextants with the model, we took the maximum value of the six probabilities of sextants located in the same prostate to be the probability of prostate cancer and used it to compare the diagnostic power of the different predictive models.

To compare the accuracy of any pair of those predictive models, the AUCs were compared by using an algorithm (11). All P values $< .05$ were considered to indicate a significant difference.

Individual relative measure of risk for each one of the variables, MR imaging (dichotomized and five-point scale), MR spectroscopy (dichotomized and five-point scale), and free-to-total PSA ratio, was obtained from the corresponding odds ratios estimated by using logistic regression. Statistical analyses were performed with statistical software (Stata 9.0; Stata, College Station, Tex).

Results

Prostate cancer was detected in 44% (24 of 54) of patients after biopsy or prostatectomy analysis of pathologic data. The sensitivity, specificity, and accuracy of digital rectal examination were 50% (12 of 24), 63% (19 of 30), and 57% (31 of 54), respectively. The mean PSA level in patients with prostate cancer (7.6 ng/mL;

range, 4.1–14.2 ng/mL) was slightly but significantly higher than that of patients without prostate cancer (6.3 ng/mL; range, 3.0–15.0 ng/mL) ($P = .043$). The mean free-to-total PSA ratio in patients with prostate cancer (11.1%; range, 6.3%–20.0%) was significantly different from that in patients without prostate cancer (16.4%; range, 8.5%–19.2%) ($P < .001$). The diagnostic accuracy of PSA level and free-to-total PSA ratio was 66.8% and 82.5%, respectively.

Figure 3

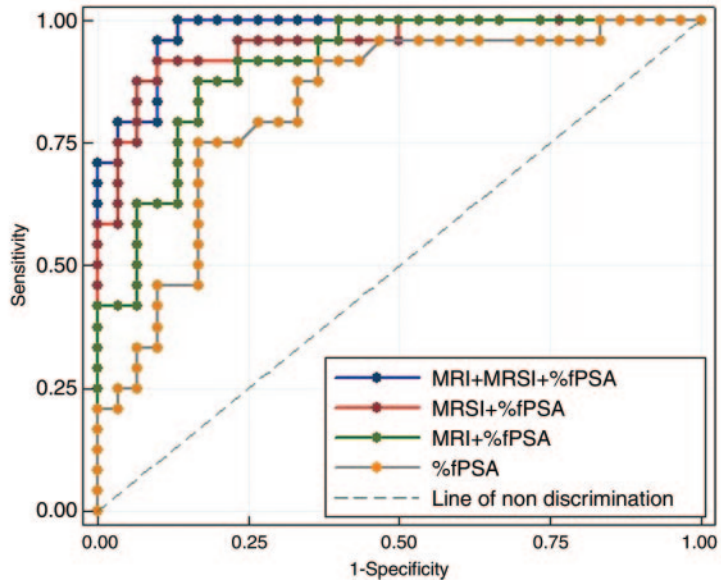

Figure 3: ROC curves for different combinations of the predictive variables: MR imaging *(MRI)*, MR spectroscopy *(MRSI)*, and free-to-total PSA ratio *(%fPSA)*. The overall accuracy of each model (97.5% for MR imaging + MR spectroscopy + free-to-total PSA ratio, 95.1% for MR spectroscopy + free-to-total PSA ratio, 90.8% for MR imaging + free-to-total PSA ratio, and 82.5% for free-to-total PSA ratio) is specified in the AUCs.

Figure 4

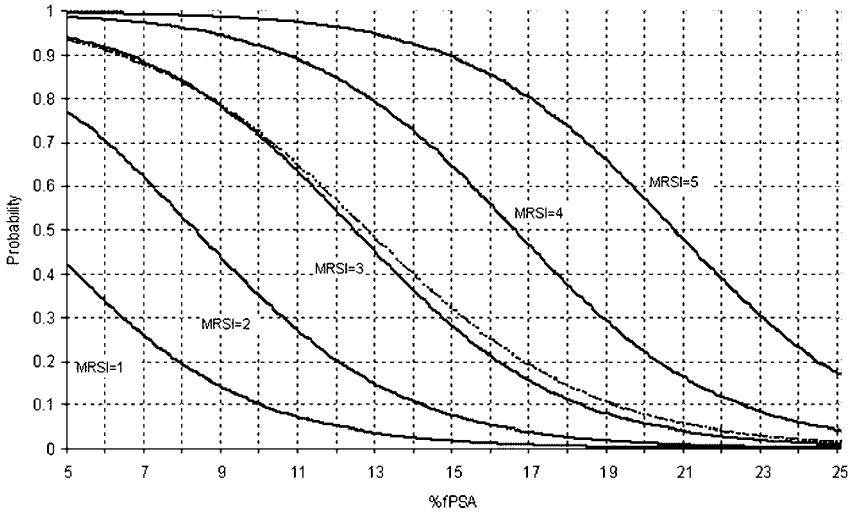

Figure 4: Graph of predictive probabilities of prostate cancer estimated from binary regression models using free-to-total PSA ratio *(%fPSA)* alone as predictive variable (dotted line) and also combined with MR spectroscopy score (*MRSI*-labeled lines).

The accuracy of the dichotomized MR imaging and MR spectroscopy prostate scores was 75.9% (41 of 54) and 90.7% (49 of 54), respectively. The accuracy of dichotomized MR spectroscopy was significantly greater than that of dichotomized MR imaging ($P = .043$). The accuracy of MR imaging and MR spectroscopy prostate scores with use of the five-point scale as predictive variables was 85.1% and 87.2%, respectively (Table 1). The accuracy of the predictive models including MR plus MR spectroscopy, free-to-total PSA ratio plus MR imaging, free-to-total PSA ratio plus MR spectroscopy, and free-to-total PSA ratio plus MR plus MR spectroscopy as predictor variables was 94.9%, 90.8%, 95.1%, and 97.5%, respectively (Table 1).

The accuracy of the complete model, including the three predictive variables of free-to-total PSA ratio, MR imaging (five-point scale), and MR spectroscopy (five-point scale), was 97.5%. This is significantly higher than the accuracy of the models using only free-to-total PSA ratio (82.5%, $P = .006$), only MR imaging (85.1%, $P = .007$), or only MR spectroscopy (87.2%, $P = .041$) as the predictive variable and also higher than the accuracy of the model using free-to-total PSA ratio and MR imaging together (90.8%, $P = .038$). Figure 2 shows MR imaging and MR spectroscopic imaging of prostate cancer, which was clearly depicted at MR spectroscopy. However the accuracy of the predictive model of free-to-total PSA ratio plus MR imaging plus MR spectroscopy (97.5%) is not significantly higher than that of the model combining MR imaging plus MR spectroscopy (94.9%, $P = .261$) or free-to-total PSA ratio plus MR spectroscopy (95.1%, $P = .290$) (Fig 3). Figure 4 shows the predictive probabilities of prostate cancer estimated from binary regression models using the free-to-total PSA ratio alone as predictive variable and also combined with MR spectroscopy prostate score.

The accuracy of the predictive model based on the generalized estimated equations approach using free-to-total PSA ratio and the individual readings of MR and MR

spectroscopy on the peripheral sextants for each prostate as predictor variables was 97.0% for exchangeable correlation structure. This accuracy is not significantly different from the accuracy (97.5%) of the predictive model that included free-to-total PSA ratio plus MR imaging plus MR spectroscopy ($P = .690$). The same generalized estimated equations predictive model for unstructured correlation structure was nonconvergent.

Table 2 gives the individual odds ratio of each predictive variable. The estimated odds ratio of the dichotomized MR imaging was 9.7. Therefore, the odds of prostate cancer when the MR score is in the range 3–5 are almost 10 times greater than when the score is in the range 1–2. Similarly, the odds of prostate cancer when MR spectroscopy scores are in the range 3–5 are almost 100 times greater than when score is in the range 1–2. Since the standard errors of these estimated odds ratios are very high, the numerical interpretations are only a way of guidance. The estimated odds ratios of the five-point scale MR and MR spectroscopy are 3.8 and 4.5, respectively. Therefore, an increase of one unit in the MR score multiplies the odds of prostate cancer by 3.8. Finally, the odds ratio of free-to-total PSA ratio is 0.7. This means that a decrease of one unit in the free-to-total PSA ratio multiplies the odds of prostate cancer by 1.4 (1 ÷ 0.7). It is important to emphasize that those individual odds ratios are all significantly different from 1, even when they are simultaneously present in the predictive model (all P values are $< .030$).

Table 2

Odds Ratios for Each Predictive Variable

Variable	Odds Ratio	*P* Value
MR imaging (dichotomized)	9.7 (2.8, 34.1)	<.001
MR spectroscopic imaging (dichotomized)	93.0 (15.0, 640.0)	<.001
MR imaging (five-point scale)	3.8 (1.8, 8.0)	<.001
MR spectroscopic imaging (five-point scale)	4.5 (2.3, 8.7)	<.001
Free-to-total PSA ratio	0.7 (0.6, 0.9)	.001

Note.—Numbers in parentheses are 95% confidence intervals.

Discussion

Our study shows a potential benefit of including MR and MR spectroscopy in the diagnostic work-up of patients with elevated PSA level and low free-to-total PSA ratio to detect prostate cancer before transrectal US-guided biopsy. A better accuracy is obtained by combining the data of MR imaging, MR spectroscopy, and free-to-total PSA ratio, although in the application of the parsimonious principle, a predictive model combining only MR spectroscopy and free-to-total PSA ratio data would be also acceptable without a significant loss of diagnostic accuracy. However, an optimized spectroscopic examination, MR spectroscopy, requires the combined morphologic data of MR imaging in order to perform an integrated analysis of the prostate.

Previous studies have shown the benefit of adding MR spectroscopy data to the information obtained at MR imaging (5,6,9,12,13), although the accuracy of the technique reported in these studies varies, especially due to the different criteria used for patient preselection and the methods used for analysis. Our study used both sextant localization and prostate localization for the analysis. Moreover, we analyzed each of these methods by using both dichotomized scores and five-point scales. Our approach yielded different accuracy for different methods; this highlights the difficulty of comparing results from previous studies. The accuracy of MR spectroscopy was 90.7% when a dichotomized score was used and 87.2% when a five-point scale was used. We confirm the benefit of including both MR imaging and MR spectroscopy in the diagnostic algorithm: Combing the two techniques significantly improves accuracy, from 85.1% and 87.2%, respectively, for MR and MR spectroscopy alone to 94.9% when they are combined. On the other hand, Costouros et al (14) recently found that the addition of MR spectroscopy to MR imaging did not significantly improve diagnostic accuracy for prostate cancer detection; nevertheless, they conclude that MR spectroscopy is a useful supplement in the diagnosis of prostate cancer. MR spectroscopy has also proved useful in conjunction with transrectal US, where transferring the metabolic data to the US images improves determination of prostate cancer (15).

Figure 5

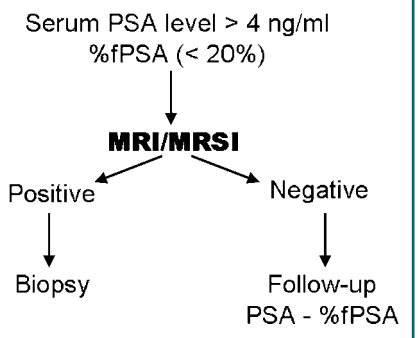

Figure 5: Flow chart for early detection of prostate cancer based on MR imaging and MR spectroscopy *(MRSI)* findings and free-to-total PSA ratio *(%fPSA)*.

We confirm the low accuracy of digital rectal examination and PSA values in detecting prostate cancer (16), although these methods are still the most widely used. We found the free-to-total PSA ratio more accurate in detecting prostate cancer, as reported elsewhere (17). Our study demonstrates the benefit of combining the clinical data (free-to-total PSA ratio) with the imaging data (MR imaging and MR spectroscopy) for detecting prostate cancer early. Our predictive model shows that for any value of free-to-total PSA ratio, the predictive probability of prostate cancer increases significantly if MR spectroscopy score is equal to 4 or 5 and decreases if it is equal to 1 or 2.

Although one recent study demonstrated improved accuracy by combining MR imaging and PSA density (18), we report on an accurate predictive model that combines MR imaging, MR spectroscopy, and free-to-total PSA ratio for de-

tecting prostate cancer. Use of MR spectroscopy could be more accurate than the current transrectal US-guided blind biopsy method, where reported data have shown prostate cancer in 20% of the patients (19).

We could further refine the algorithm to detect prostate cancer by incorporating free-to-total PSA ratio data early on. Patients with PSA between 4.0 and 10 ng/mL and a low free-to-total PSA ratio could be examined with MR imaging plus MR spectroscopy to determine whether biopsy is necessary (Fig 5). Positive results at MR imaging plus MR spectroscopy would call for transrectal US-guided biopsy, and the metabolic data could be accurately transferred to the transrectal US images to help guide biopsy (15). Whether cancer detection rates improve significantly with extensive saturation-biopsy regimens is arguable; however, morbidity in these regimens is clearly higher (20). Performing biopsy on the target lesion detected at MR spectroscopy would be more accurate than using the current blind biopsy method, and the indication for biopsy would be more efficient than use of current methods based on digital rectal examination findings and PSA values. Thus, performing prostate biopsy with use of MR and MR spectroscopy data could improve the biopsy detection rate of prostate cancer. However, the method we propose requires a high level of expertise in MR spectroscopy and prostatic biopsy targeting. Moreover, the software and the acquisition techniques vary with different vendors, and while some MR imagers allow the study to be performed with a surface coil, others require an endorectal coil (21).

We also found improved accuracy with MR imaging and free-to-total PSA ratio combined (90.8%) than with either technique alone. We have confirmed the moderate accuracy of using MR imaging alone, as previously reported (22–24). Finally, it is important to note that MR imaging and MR spectroscopy findings for some benign conditions, especially chronic prostatitis, can be similar to findings for prostate cancer (25).

Certain limitations and drawbacks of our study and the proposed prostate cancer detection algorithm should be mentioned. First, MR spectroscopy is not widely available. Second, a better standardized scoring system must be developed to enable MR spectroscopy to be widely used, although one report shows good accuracy with use of a standardized five-point scale (26). Third, our patients were selected without prior biopsies; however, MR spectroscopy is routinely used in patients with previous negative biopsy findings. Fourth, we only analyzed the peripheral zone because we considered the prostate gland as a unit to enable us to analyze the imaging results in combination with the clinical data, which always refer to the whole gland. Moreover, the metabolic ratios of the peripheral and central gland are considered different to be analyzed as a whole unit. A main limitation of our study was the correlation of the imaging with the pathologic findings: Only 11 patients underwent prostatectomy, so the imaging-histologic correlation in the remaining 44 patients could only be performed with biopsy results. Therefore, we have to consider that because of the low sensitivity of transrectal US-guided biopsy as a standard of reference, it is possible that some patients who had negative biopsy findings could in fact had cancer. For this reason, all of the 30 patients with negative biopsy findings have been followed up. The data from those patients are being evaluated and will be reported. The difficulty of correlating the MR imaging or MR spectroscopy findings with biopsy results and even with surgical specimens is well known from attempts to ensure the correspondence of transrectal US-guided biopsy to suspicious areas on MR or MR spectroscopic images (10,27). Finally, our series of patients was small (n = 54) and larger studies are necessary to better assess these preliminary results.

In conclusion, combining data from MR imaging, MR spectroscopy, and free-to-total PSA ratio could improve prostate cancer detection in patients suspected of having prostate cancer and could obviate a substantial number of unnecessary biopsies.

Acknowledgment: The authors thank John Giba, BS, for help with the English language.

References

1. Thompson IM, Pauler DK, Goodman PJ, et al. Prevalence of prostate cancer among men with a prostate-specific antigen level ≤ 4.0 ng per milliliter. N Engl J Med 2004;350:2239–2246.
2. Arcangeli CG, Ornstein DK, Keetch DW, Andriole GL. Prostate-specific antigen as a screening test for prostate cancer: the United States experience. Urol Clin North Am 1997;24:299–306.
3. Andriole GL, Catalona WJ. Using PSA to screen for prostate cancer: the Washington University experience. Urol Clin North Am 1993;20:647–651.
4. Wefer AE, Hricak H, Vigneron DB, et al. Sextant localization of prostate cancer: comparison of sextant biopsy, magnetic resonance imaging and magnetic resonance spectroscopic imaging with step section histology. J Urol 2000;164:400–404.
5. Yu KK, Scheidler J, Hricak H, et al. Prostate cancer: prediction of extracapsular extension with endorectal MR imaging and three-dimensional proton MR spectroscopic imaging. Radiology 1999;213:481–488.
6. Scheidler J, Hricak H, Vigneron DB, et al. Prostate cancer: localization with three-dimensional proton MR spectroscopic imaging—clinicopathologic study. Radiology 1999;213:473–480.
7. Shah JB, Reese AC, McKiernan JM, Benson MC. PSA updated: still relevant in the new millennium? Eur Urol 2005;47:427–432.
8. Roddam AW, Duffy MJ, Hamdy FC, et al. Use of prostate-specific antigen (PSA) isoforms for the detection of prostate cancer in men with a PSA level of 2–10 ng/ml: systematic review and meta-analysis. Eur Urol 2005;48:386–399.
9. Kurhanewicz J, Vigneron DB, Hricak H, Narayan P, Carroll P, Nelson SJ. Three-dimensional H-1 MR spectroscopic imaging of the in situ human prostate with high (0.24–0.7-cm3) spatial resolution. Radiology 1996;198:795–805.
10. Futterer JJ, Heijmink SW, Scheenen TW, et al. Prostate cancer localization with dynamic contrast-enhanced MR imaging and proton MR spectroscopic imaging. Radiology 2006;241:449–458.
11. DeLong ER, DeLong DM, Clarke-Pearson DL. Comparing the areas under two or more correlated receiver operating characteristic curves: a nonparametric approach. Biometrics 1988;44:837–845.

12. Coakley FV, Kurhanewicz J, Lu Y, et al. Prostate cancer tumor volume: measurement with endorectal MR and MR spectroscopic imaging. Radiology 2002;223:91–97.

13. Mueller-Lisse UG, Vigneron DB, Hricak H, et al. Localized prostate cancer: effect of hormone deprivation therapy measured by using combined three-dimensional ^{1}H MR spectroscopy and MR imaging: clinicopathologic case-controlled study. Radiology 2001; 221:380–390.

14. Costouros NG, Coakley FV, Westphalen AC, et al. Diagnosis of prostate cancer in patients with an elevated prostate-specific antigen level: role of endorectal MRI and MR spectroscopic imaging. AJR Am J Roentgenol 2007;188:812–816.

15. Prando A, Kurhanewicz J, Borges AP, Oliveira EM Jr, Figueiredo E. Prostatic biopsy directed with endorectal MR spectroscopic imaging findings in patients with elevated prostate specific antigen levels and prior negative biopsy findings: early experience. Radiology 2005;236:903–910.

16. Catalona WJ, Richie JP, Ahmann FR, et al. Comparison of digital rectal examination and serum prostate specific antigen in the early detection of prostate cancer: results of a multicenter clinical trial of 6,630 men. J Urol 1994;151:1283–1290.

17. Okegawa T, Noda H, Nutahara K, Higashihara E. Comparisons of the various combinations of free, complexed, and total prostate-specific antigen for the detection of prostate cancer. Eur Urol 2000;38:380–387.

18. Kubota Y, Kamei S, Nakano M, Ehara H, Deguchi T, Tanaka O. The potential role of prebiopsy magnetic resonance imaging combined with prostate-specific antigen density in the detection of prostate cancer. Int J Urol 2008;15:322–326.

19. Keetch DW, Catalona WJ, Smith DS. Serial prostatic biopsies in men with persistently elevated serum prostate specific antigen values. J Urol 1994;151:1571–1574.

20. Simon J, Kuefer R, Bartsch G Jr, Volkmer BG, Hautmann RE, Gottfried HW. Intensifying the saturation biopsy technique for detecting prostate cancer after previous negative biopsies: a step in the wrong direction. BJU Int 2008;102:459–462.

21. Akin O, Hricak H. Imaging of prostate cancer. Radiol Clin North Am 2007;45:207–222.

22. Vilanova JC, Comet J, Capdevila A, et al. The value of endorectal MR imaging to predict positive biopsies in clinically intermediate-risk prostate cancer patients. Eur Radiol 2001;11:229–235.

23. Yu KK, Hricak H. Imaging prostate cancer. Radiol Clin North Am 2000;38:59–85, viii.

24. Hricak H, White S, Vigneron D, et al. Carcinoma of the prostate gland: MR imaging with pelvic phased-array coils versus integrated endorectal–pelvic phased-array coils. Radiology 1994;193:703–709.

25. Shukla-Dave A, Hricak H, Eberhardt SC, et al. Chronic prostatitis: MR imaging and 1H MR spectroscopic imaging findings—initial observations. Radiology 2004;231:717–724.

26. Jung JA, Coakley FV, Vigneron DB, et al. Prostate depiction at endorectal MR spectroscopic imaging: investigation of a standardized evaluation system. Radiology 2004;233: 701–708.

27. Hom JJ, Coakley FV, Simko JP, et al. Prostate cancer: endorectal MR imaging and MR spectroscopic imaging—distinction of true-positive results from chance-detected lesions. Radiology 2006;238:192–199.

Radiology 2009

This is your reprint order form or pro forma invoice

(Please keep a copy of this document for your records.)

Reprint order forms and purchase orders or prepayments must be received 72 hours after receipt of form either by mail or by fax at 410-820-9765. It is the policy of Cadmus Reprints to issue one invoice per order. **Please print clearly**.

Author Name _____
Title of Article _____
Issue of Journal_____ Reprint # _____ Publication Date _____
Number of Pages_____ KB # _____ Symbol Radiology
Color in Article? Yes / No (Please Circle)

Please include the journal name and reprint number or manuscript number on your purchase order or other correspondence.

Order and Shipping Information

Reprint Costs **(Please see page 2 of 2 for reprint costs/fees.)**

_____ Number of reprints ordered $_____
_____ Number of color reprints ordered $_____
_____ Number of covers ordered $_____
Subtotal $_____
Taxes $_____

(*Add appropriate sales tax for Virginia, Maryland, Pennsylvania, and the District of Columbia or Canadian GST to the reprints if your order is to be shipped to these locations*.)

First address included, add $32 for each additional shipping address $_____

TOTAL $_____

Shipping Address **(cannot ship to a P.O. Box) Please Print Clearly**

Name _____
Institution _____
Street _____
City _____ State _____ Zip _____
Country _____
Quantity_____ Fax _____
Phone: Day _____ Evening _____
E-mail Address _____

Additional Shipping Address* **(cannot ship to a P.O. Box)**

Name _____
Institution _____
Street _____
City _____ State _____ Zip _____
Country _____
Quantity _____ Fax _____
Phone: Day _____ Evening _____
E-mail Address _____

** Add $32 for each additional shipping address*

Payment and Credit Card Details

Enclosed: Personal Check _____
Credit Card Payment Details _____

Checks must be paid in U.S. dollars and drawn on a U.S. Bank.

Credit Card: __ VISA __ Am. Exp. __ MasterCard
Card Number _____
Expiration Date_____
Signature: _____

Please send your order form and prepayment made payable to:

Cadmus Reprints
P.O. Box 751903
Charlotte, NC 28275-1903

Note: Do not send express packages to this location, PO Box.

FEIN #:541274108

Invoice or Credit Card Information

Invoice Address **Please Print Clearly**

Please complete Invoice address as it appears on credit card statement

Name _____
Institution _____
Department _____
Street _____
City _____ State _____ Zip _____
Country _____
Phone _____ Fax _____
E-mail Address _____

Cadmus will process credit cards and *Cadmus Journal Services* will appear on the credit card statement.

If you don't mail your order form, you may fax it to 410-820-9765 with your credit card information.

Signature _____ Date _____

Signature is required. By signing this form, the author agrees to accept the responsibility for the payment of reprints and/or all charges described in this document.

RB-1/01/09

Radiology 2009

Black and White Reprint Prices

Domestic (USA only)						
# of Pages	50	100	200	300	400	500
1-4	$239	$260	$285	$303	$323	$340
5-8	$379	$420	$455	$491	$534	$572
9-12	$507	$560	$651	$684	$748	$814
13-16	$627	$698	$784	$868	$954	$1,038
17-20	$755	$845	$947	$1,064	$1,166	$1,272
21-24	$878	$985	$1,115	$1,250	$1,377	$1,518
25-28	$1,003	$1,136	$1,294	$1,446	$1,607	$1,757
29-32	$1,128	$1,281	$1,459	$1,632	$1,819	$2,002
Covers	$149	$164	$219	$275	$335	$393

International (includes Canada and Mexico)						
# of Pages	50	100	200	300	400	500
1-4	$299	$314	$367	$429	$484	$546
5-8	$470	$502	$616	$722	$838	$949
9-12	$637	$687	$852	$1,031	$1,190	$1,369
13-16	$794	$861	$1,088	$1,313	$1,540	$1,765
17-20	$963	$1,051	$1,324	$1,619	$1,892	$2,168
21-24	$1,114	$1,222	$1,560	$1,906	$2,244	$2,588
25-28	$1,287	$1,412	$1,801	$2,198	$2,607	$2,998
29-32	$1,441	$1,586	$2,045	$2,499	$2,959	$3,418
Covers	$211	$224	$324	$444	$558	$672

Color Reprint Prices

Domestic (USA only)						
# of Pages	50	100	200	300	400	500
1-4	$247	$267	$385	$515	$650	$780
5-8	$297	$435	$655	$923	$1194	$1467
9-12	$445	$563	$926	$1,339	$1,748	$2,162
13-16	$587	$710	$1,201	$1,748	$2,297	$2,843
17-20	$738	$858	$1,474	$2,167	$2,846	$3,532
21-24	$888	$1,005	$1,750	$2,575	$3,400	$4,230
25-28	$1,035	$1,164	$2,034	$2,986	$3,957	$4,912
29-32	$1,186	$1,311	$2,302	$3,402	$4,509	$5,612
Covers	$149	$164	$219	$275	$335	$393

International (includes Canada and Mexico))						
# of Pages	50	100	200	300	400	500
1-4	$306	$321	$467	$642	$811	$986
5-8	$387	$517	$816	$1,154	$1,498	$1,844
9-12	$574	$689	$1,157	$1,686	$2,190	$2,717
13-16	$754	$874	$1,506	$2,193	$2,883	$3,570
17-20	$710	$1,063	$1,852	$2,722	$3,572	$4,428
21-24	$1,124	$1,242	$2,195	$3,231	$4,267	$5,300
25-28	$1,320	$1,440	$2,541	$3,738	$4,957	$6,153
29-32	$1,498	$1,616	$2,888	$4,269	$5,649	$7028
Covers	$211	$224	$324	$444	$558	$672

Minimum order is 50 copies. For orders larger than 500 copies, please consult Cadmus Reprints at 800-407-9190.

Reprint Cover

Cover prices are listed above. The cover will include the publication title, article title, and author name in black.

Shipping

Shipping costs are included in the reprint prices. Domestic orders are shipped via FedEx Ground service. Foreign orders are shipped via a proof of delivery air service.

Multiple Shipments

Orders can be shipped to more than one location. Please be aware that it will cost $32 for each additional location.

Delivery

Your order will be shipped within 2 weeks of the journal print date. Allow extra time for delivery.

Tax Due

Residents of Virginia, Maryland, Pennsylvania, and the District of Columbia are required to add the appropriate sales tax to each reprint order. For orders shipped to Canada, please add 7% Canadian GST unless exemption is claimed.

Ordering

Reprint order forms and purchase order or prepayment is required to process your order. Please reference journal name and reprint number or manuscript number on any correspondence. You may use the reverse side of this form as a proforma invoice. Please return your order form and prepayment to:

Cadmus Reprints
P.O. Box 751903
Charlotte, NC 28275-1903

Note: Do not send express packages to this location, PO Box.
FEIN #:541274108

Please direct all inquiries to:

Rose A. Baynard
800-407-9190 (toll free number)
410-819-3966 (direct number)
410-820-9765 (FAX number)
baynardr@cadmus.com (e-mail)

Reprint Order Forms and purchase order or prepayments must be received 72 hours after receipt of form.